



Injury-induced myosin-specific tissue-resident memory T cells drive immune checkpoint inhibitor myocarditis

Hannah Kalinoski^a , Abdel Daoud^a, Vitali Rusinevich^b , Ivana Jurčová^c, Monica V. Talor^b, Robin A. Welsh^b, David Hughes^{b,d}, Kateřina Zemanová^e, Ilja Stržíž^e, Jody E. Hooper^{b,1}, Josef Kautzner^c, Petr Pejchal^c , Vojtěch Melenovský^c , Taejoon Won^{b,2,3}, and Daniela Čiháková^{a,b,3,4}

Affiliations are included on p. 11.

Edited by John O'Shea, National Institute of Arthritis and Musculoskeletal and Skin Diseases, Bethesda, MD; received January 21, 2024; accepted September 10, 2024

Cardiac myosin-specific (MyHC) T cells drive the disease pathogenesis of immune checkpoint inhibitor–associated myocarditis (ICI-myocarditis). To determine whether MyHC T cells are tissue-resident memory T (T_{RM}) cells, we characterized cardiac T_{RM} cells in naïve mice and established that they have a distinct phenotypic and transcriptional profile that can be defined by their upregulation of CD69, PD-1, and CXCR6. We then investigated the effects of cardiac injury through a modified experimental autoimmune myocarditis mouse model and an ischemia–reperfusion injury mouse model and determined that cardiac inflammation induces the recruitment of autoreactive MyHC T_{RM} cells, which coexpress PD-1 and CD69. To investigate whether the recruited MyHC T_{RM} cells could increase susceptibility to ICI-myocarditis, we developed a two-hit ICI-myocarditis mouse model where cardiac injury was induced, mice were allowed to recover, and then were treated with anti-PD-1 antibodies. We determined that mice who recover from cardiac injury are more susceptible to ICI-myocarditis development. We found that murine and human T_{RM} cells share a similar location in the heart and aggregate along the perimyocardium. We phenotyped cells obtained from pericardial fluid from patients diagnosed with dilated cardiomyopathy and ischemic cardiomyopathy and established that pericardial T cells are predominantly CD69⁺ T_{RM} cells that up-regulate PD-1. Finally, we determined that human pericardial macrophages produce IL-15, which supports and maintains pericardial T_{RM} cells.

tissue-resident memory T cells | ICI-myocarditis | PD-1 | cardiac immunology

Immune checkpoint molecules such as cytotoxic T lymphocyte-associated protein 4 (CTLA-4) and programmed cell death protein 1 (PD-1) are negative regulators of T cell activation (1–4). The development of immune checkpoint inhibitor (ICI) therapies has proven to reinvigorate exhausted tumor-infiltrating lymphocytes (TIL), though clinically efficacious, 40 to 72% of patients go on to develop immune-related adverse events (irAE) (5–8). While most irAEs are mild to moderate in clinical severity, inflammation of the heart muscle, or myocarditis, is the deadliest irAE (7). ICI-associated myocarditis (ICI-myocarditis) predominately affects patients treated with antibodies blocking the PD-1/PD-L1 axis and is a rare irAE that affects less than 1% of patients but has a mortality rate of up to 50% (7–10). Due to the high fatality rate, it is imperative to understand what predisposes patients to develop ICI-myocarditis. Our lab and others recently showed that ICI-myocarditis is mediated by autoreactive T cells specific for the α -heavy chain of cardiac myosin (11, 12). Further characterization of these cardiac myosin-specific (MyHC) T cells revealed an antigen-experienced phenotype and expression of CD69 (11, 12). Upregulation of CD69 has been associated with T cell activation and tissue residency (13–15).

Murine T cells can be separated into functionally distinct subsets with memory T cells distinguished by their expression of the activation marker CD44 (14, 15). In comparison, naïve T (T_N) cells are antigen inexperienced and, as such, have yet to be activated. T_N cells and central memory T (T_{CM}) cells are defined by their ability to enter the secondary lymphoid organs. To do this, they express lymph node homing molecules such as CCR7 and CD62L (14, 15). In contrast, effector memory T (T_{EM}) cells survey the peripheral tissues and do not express lymph node homing molecules (14, 15). Tissue-resident memory T (T_{RM}) cells are the most recently discovered subset of memory T cells; they are noncirculating and remain resident in the peripheral tissues (14–16). CD69 and CD103 are classical T_{RM} cell markers that help maintain tissue residency (14, 15, 17). CD69 is an early activation marker that directly antagonizes the tissue egress protein, sphingosine 1-phosphate receptor 1 (S1PR1) (18, 19). Another classical marker for T_{RM} cells is CD103, which dimerizes with integrin β 7 to bind E-cadherin and is important for retention in

Significance

We determined that cardiac MyHC T_{RM} cells are present in naïve hearts and accumulate in the pericardial area in mice and humans after recovering from cardiac injury. T_{RM} cells express high levels of PD-1, making them susceptible to activation by anti-PD-1 blocking antibodies. ICI-myocarditis is more prevalent after previous cardiac injury, demonstrating that T_{RM} cells perpetuate the disease. Thus, our results provide unique insights into risk factors and the disease pathogenesis of ICI-myocarditis.

Author contributions: H.K., P.P., V.M., T.W., and D.C. designed research; H.K., A.D., V.R., I.J., M.V.T., R.A.W., D.H., K.Z., I.S., J.E.H., J.K., P.P., V.M., and T.W. performed research; H.K. and A.D. analyzed data; and H.K. and D.C. wrote the paper.

Competing interest statement: Dr. Čiháková has research grants with CSL Behring and Cantargia. Neither grant conflicts with this project.

This article is a PNAS Direct Submission.

Copyright © 2024 the Author(s). Published by PNAS. This article is distributed under Creative Commons Attribution-NonCommercial-NoDerivatives License 4.0 (CC BY-NC-ND).

¹Present address: Department of Pathobiology, Stanford University School of Medicine.

²Present address: Department of Pathobiology, University of Illinois.

³To whom correspondence may be addressed. Email: twon@illinois.edu or Cihakova@jhmi.edu.

⁴D.C. contributed equally to this work.

This article contains supporting information online at <https://www.pnas.org/lookup/suppl/doi:10.1073/pnas.2323052121/-DCSupplemental>.

Published October 8, 2024.

epithelial tissues (14, 20). T_{RM} cells have been shown to accumulate in the tissues after injury or vaccination, where they become long-lived resident immune cells (21–24). T_{RM} cells act as a first-line defense against invading pathogens in the peripheral tissues by coordinating innate and adaptive immune responses (25–27). Though initially described for their protective qualities, T_{RM} cells have also been implicated in the pathogenesis of certain autoimmune diseases such as psoriasis and vitiligo (28, 29). In addition, it has been shown that T_{RM} cells express high levels of PD-1 and use the PD-1/PD-L1 axis to maintain tissue homeostasis (30, 31). Currently, T_{RM} cells have been characterized in a variety of tissues but have yet to be defined in the heart.

Autoreactive cardiac myosin-specific T cells have been shown to escape negative selection in the thymus and can be found in the periphery (32). Our previous studies have shown that myosin-specific T cells are located in the hearts of naive mice (11). Furthermore, our lab, as well as others, has shown that myosin-specific T cells are recruited to the heart during cardiovascular disease and can play both pathogenic and protective roles (11, 33, 34). Currently, it remains unclear whether these recruited autoreactive MyHCT cells maintain long-term residency in the heart and what function they play. In this manuscript, we describe the contribution of cardiac T_{RM} cells in the disease pathogenesis of ICI-myocarditis. We demonstrate that murine mouse models of cardiac injury induce the recruitment of autoreactive cardiac myosin-specific CD69⁺PD-1⁺T_{RM} cells into the heart, which preferentially locate along the perimyocardium. To investigate the contribution of MyHC T_{RM} cells to ICI-myocarditis development, we created a two-hit ICI-myocarditis mouse model and showed that mice who recover from previous cardiac injury are more susceptible to ICI-myocarditis development. Finally, we demonstrated that human patients diagnosed with various cardiovascular diseases have pericardial CD69⁺T_{RM} cells that up-regulate the expression of PD-1, which match the phenotype and location of murine cardiac T_{RM} cells.

Results

CD69 and PD-1 Expression Distinguishes Cardiac T_{RM} cells. CD69 and CD103 are well-characterized tissue retention markers that distinguish T_{RM} cells in various tissues (14, 15, 17). To investigate whether these classical markers differentiate cardiac T_{RM} cells from circulating T cells, we performed multiparameter flow cytometry on hearts of naive A/J mice. T cells were stratified into T_N, T_{CM}, T_{EM}, and T_{RM} populations based on the expression of CD62L and CD44 (*SI Appendix*, Fig. S1 A and B). CD69 was differentially expressed by cardiac T_{RM} cells, while CD103 was not (*SI Appendix*, Fig. S1 C and D). To further characterize cardiac T_{RM} cells, we performed intravascular labeling on naive A/J mice, which allowed us to distinguish between infiltrating immune cells trapped in the vasculature and cardiac resident leukocytes (Fig. 1 A and B) (35). Resident cardiac T cells up-regulated CD69 in comparison to infiltrating T cells (Fig. 1C and *SI Appendix*, Fig. S1E). To further characterize resident cardiac lymphocytes, we assessed the expression of PD-1, which has been reported to be up-regulated by resident memory T cells in other organs (30, 31). First, we investigated the expression of PD-1 on infiltrating and resident T cells and found that cardiac resident T cells had significantly higher expression of PD-1 compared to infiltrating T cells (*SI Appendix*, Fig. S1 F–H). To determine whether resident T_{RM} cells up-regulate the expression of PD-1, we compared the expression of PD-1 on resident CD69⁺ and CD69⁻ T cells and found that PD-1 expression was significantly higher on resident CD69⁺ T cells (Fig. 1 D and E). Together, these findings suggest that PD-1 and CD69 are coexpressed by cardiac T_{RM} cells. Autoreactive MyHCT cells were

shown to escape negative selection in the thymus (32). To determine whether these autoreactive T cells are cardiac resident, we stained cells with a tetramer specific for the TCR, which recognizes the α -chain of cardiac myosin (MyHC α _{334–352}). Autoreactive CD4⁺ and CD8⁺ MyHC T cells were significantly increased in the resident lymphocyte population (Fig. 1 F and G). This finding indicates that autoreactive MyHC T cells maintain residency in the naive mouse heart but are also found in circulation, consistent with our previous findings (11). Autoreactive effector MyHC T cells recruited to the heart after ischemic injury have been shown to up-regulate a regulatory T cell (Treg) signature (33, 34). Tregs are defined by their expression of the transcription factor FOXP3 and the high affinity IL-2 receptor alpha (CD25) (36). To determine whether resident MyHC T cells in a naive mouse heart are Tregs, we costained for FOXP3, CD25, and the cardiac myosin-specific tetramer. We found that a majority of resident autoreactive MyHC T cells were conventional T cells (Tconv) and not Tregs (Fig. 1 H and I). Thus, cardiac T_{RM} cells, including MyHC T cells, reside in the heart during naive states and are characterized by their expression of CD69 and upregulation of PD-1.

Cardiac T_{RM} Cells are Transcriptionally Distinct from Peripheral T Cells. To determine whether cardiac T_{RM} cells have a distinct transcriptional profile compared to peripheral T cells, we used fluorescence-activated cell sorting (FACS) to isolate circulating T_N, T_{CM}, T_{EM}, and cardiac CD69⁺ T_{RM} cells from naive A/J mice and then performed RT-qPCR (cell sorting gating strategy in *SI Appendix*, Fig. S2 A and B). We then plotted the generated CT values as a ratio over the housekeeping gene GAPDH, therefore, transcripts with higher expression have a lower ratio. We investigated whether cardiac T_{RM} cells down-regulate the tissue egress protein S1PR1, which is known to be suppressed by CD69 as a mechanism for cells to maintain residency in peripheral tissues (18, 19). We found that cardiac T_{RM} cells did not alter the expression of S1pr1 but had a low, or nondetectable expression, of S1pr5 (*SI Appendix*, Fig. S2C). We then examined the gene expression of the activation marker PD-1 (*Pdcd1*) and the chemokine receptor Cxcr6 and found that cardiac T_{RM} cells up-regulated both compared to circulating T cells (Fig. 2A). Finally, T_{RM} cells are known to have altered metabolism and express various isoforms of the fatty acid binding proteins (FABPs), which are important for the formation and maintenance of T_{RM} cells in peripheral tissues such as the skin and the liver (37, 38). Of the nine isoforms, we found that cardiac T_{RM} cells up-regulated the expression of three isoforms: *Fabp3*, *Fabp4*, and *Pmp2* (Fig. 2A).

To validate our RT-qPCR findings, we analyzed a publicly available single-cell RNA sequencing dataset of murine cardiac leukocytes (39). In this dataset, mice were induced with experimental autoimmune myocarditis (EAM), and at various stages of the disease, hearts were harvested, and leukocytes were sorted and run on a 10X Genomics Platform (39). Our analysis of this dataset demonstrated that cardiac T cells subclustered into T_N, T_{CM}, T_{EM}, and T_{RM} populations based on distinct gene expression profiles (Fig. 2B). We investigated the expression of T_{RM} cell markers such as CD69, PD-1, and CXCR6 and found that the expression of all these genes together were up-regulated in the cardiac T_{RM} cell subcluster (Fig. 2C). We then performed differential gene analysis and found that cardiac T_N cells exhibited the highest expression of S1pr1 and Klf2, which are responsible for tissue egress (Fig. 2 D and E and *SI Appendix*, Table S1). We found that cardiac T_{RM} cells displayed up-regulated expression of Runx3, a well-defined tissue-resident transcription factor that is important for T_{RM} cell development (40, 41) (Fig. 2 D and E). We then analyzed the expression of other immune checkpoint molecules, such as CTLA-4, TIGIT, and LAG3. We found

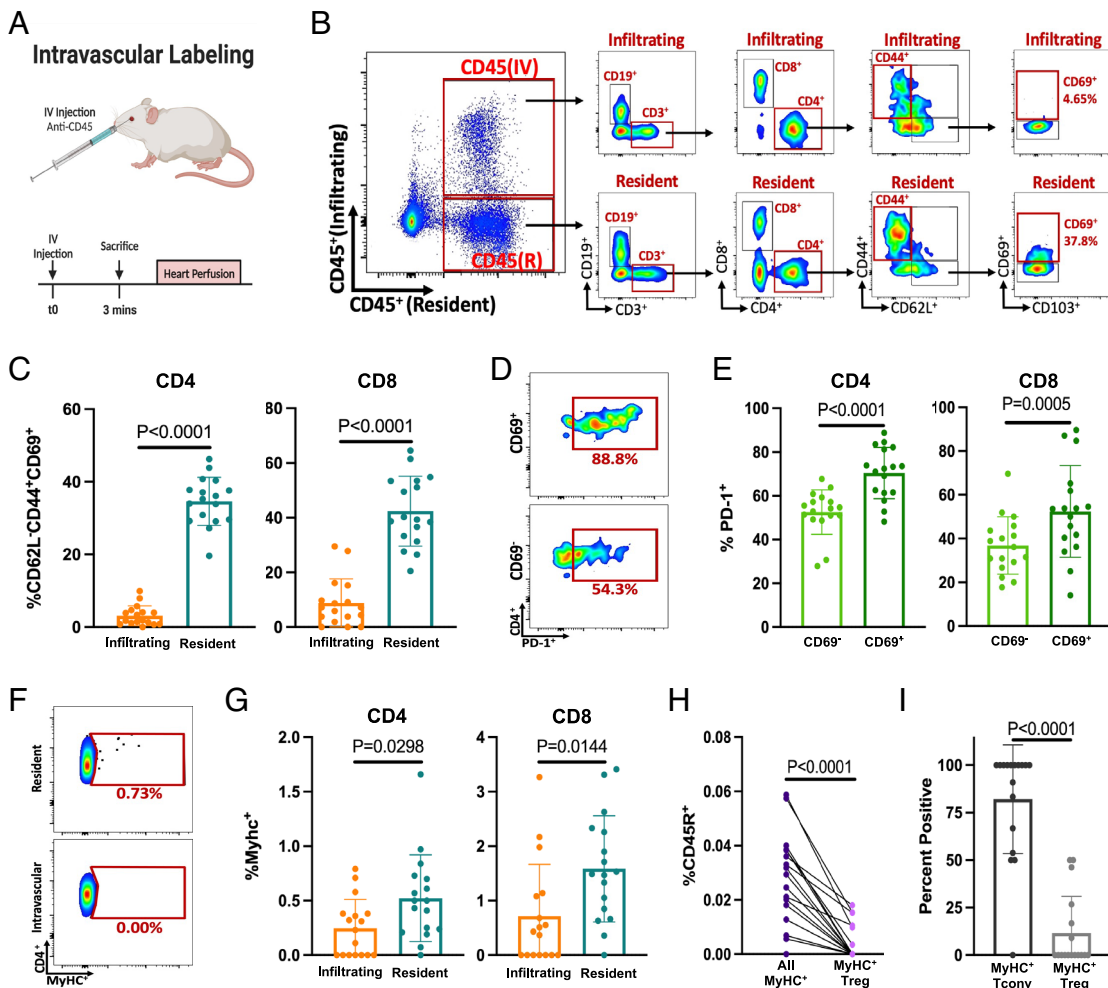


Fig. 1. CD69 and PD-1 expression distinguishes cardiac T_{RM} cells from circulating T cells. (A) Graphical depiction of the intravascular labeling technique. (B) Gating strategy for determining infiltrating and resident T cells. (C–G) Comparing the expression of CD69, PD-1, and cardiac myosin tetramer in infiltrating (CD45IV⁺) and resident (CD45IV⁺) cardiac T cells. (H) Determining the proportion of regulatory T cells (Tregs) compared to all resident myosin-specific T cells. (I) Determining the proportion of Tregs and conventional T cells (Tconv) from all resident MyHC⁺ T cells. Naive A/J male, female, young (10 wk), and aged (40 wk) mice were included in this analysis. Group size was n = 17. Statistical significance was determined through a paired t test.

that, unlike PD-1, the gene expression of the other checkpoint molecules was up-regulated by T_{CM} cells and not T_{RM} cells (Fig. 2 D and E). Subsequently, we examined effector cytokines and found that cardiac T_{RM} cells showed up-regulated gene expression of both *Tnf* and *Il17a* (Fig. 2 D and E). IL-17A has been implicated in negative cardiac remodeling during autoimmune myocarditis by our lab and others (42, 43). We then investigated the gene expression of cytokine receptors and found that cardiac T_{RM} cells up-regulated the gene expression of IL-2R β , a shared receptor for both IL-2 and IL-15 signaling (Fig. 2 D and E) (23, 44). IL-15 is part of the common γ -chain family of cytokines and is necessary for T_{RM} cell maintenance in the skin (23). Finally, to demonstrate that cardiac T_{RM} cells have a similar gene signature to other T_{RM} cells, we integrated our reanalysis of cardiac T_{RM} cells with a publicly available bulk RNA sequencing dataset of skin T_{RM} cells and spleen T_{EM} cells (17). We then developed a model that allowed us to ascribe a cardiac T_{RM} score to both the skin T_{RM} cells and the spleen T_{EM} cells. For this model, the higher the score, the more transcriptionally similar the sample is to the cardiac T_{RM} cells. We found that skin T_{RM} cells were more similar to cardiac T_{RM} cells than spleen T_{EM} cells (SI Appendix, Fig. S2D), indicating that cardiac T_{RM} cells share a gene signature that is more similar to other resident memory T cells than circulating T cells. Together, these findings indicate cardiac T_{RM} cells are transcriptionally distinct and up-regulate a T_{RM}-like signature.

Cardiac Injury and Aging Induce Autoreactive CD69⁺ T_{RM} Cells. It has been shown that pathogen exposure or localized inflammation leads to the accumulation of T_{RM} cells in various tissues (22, 23, 45). This led us to hypothesize that cardiac injury would cause the

induction of T_{RM} cells into the heart. To study this, we employed a modified EAM (mEAM) mouse model, which induces a low level of cardiac inflammation that mostly resolves after 8 wk (Fig. 3A). To characterize the phenotype of cardiac T cells throughout the model, we performed a time course experiment looking at T cells at weeks 0, 2, 3, and 8. To determine the phenotype of cardiac CD4⁺ T cells during mEAM, we first performed unbiased clustering through t-distributed stochastic neighbor embedding (t-SNE) (Fig. 3B). From the unsupervised clustering, we distinguished 9 clusters from which we assigned conventional T cell classifications (gating strategy in SI Appendix, Fig. S3A). We found that the cardiac T_{RM} cell cluster coincided with the highest expression of CD69, CD44, PD-1, and CXCR6 (Fig. 3B). We then stratified the CD4⁺ T cells based on the time course and determined that at day 0, the predominant populations were infiltrating T_N cells and T_{EM} cells (Fig. 3C). After week 8, we found that a majority of inflammation had abated and that there was a substantial increase in cardiac T_{RM} cells (Fig. 3C). These findings mirror our analysis of the publicly available conventional EAM single-cell RNA sequencing dataset, where cardiac T_{RM} cells are enriched on day 60 after EAM (SI Appendix, Fig. S3B) (39). We then quantified the proportion of CD69⁺PD-1⁺ T cells in the heart before and 8 wk after mEAM induction and found a significant increase in both CD4⁺ and CD8⁺ T_{RM} cells in mice who received mEAM (Fig. 3D and SI Appendix, Fig. S3C). We next investigated the phenotype of resident MyHC T cells in naive mice and mice who recovered from mEAM and found that all MyHC T cells expressed PD-1 and a significant portion expressed CD69 (Fig. 3E). Next, we inspected whether recovery from mEAM led to an increase in MyHC CD69⁺PD-1⁺ T_{RM} cells compared to naive mice and found a

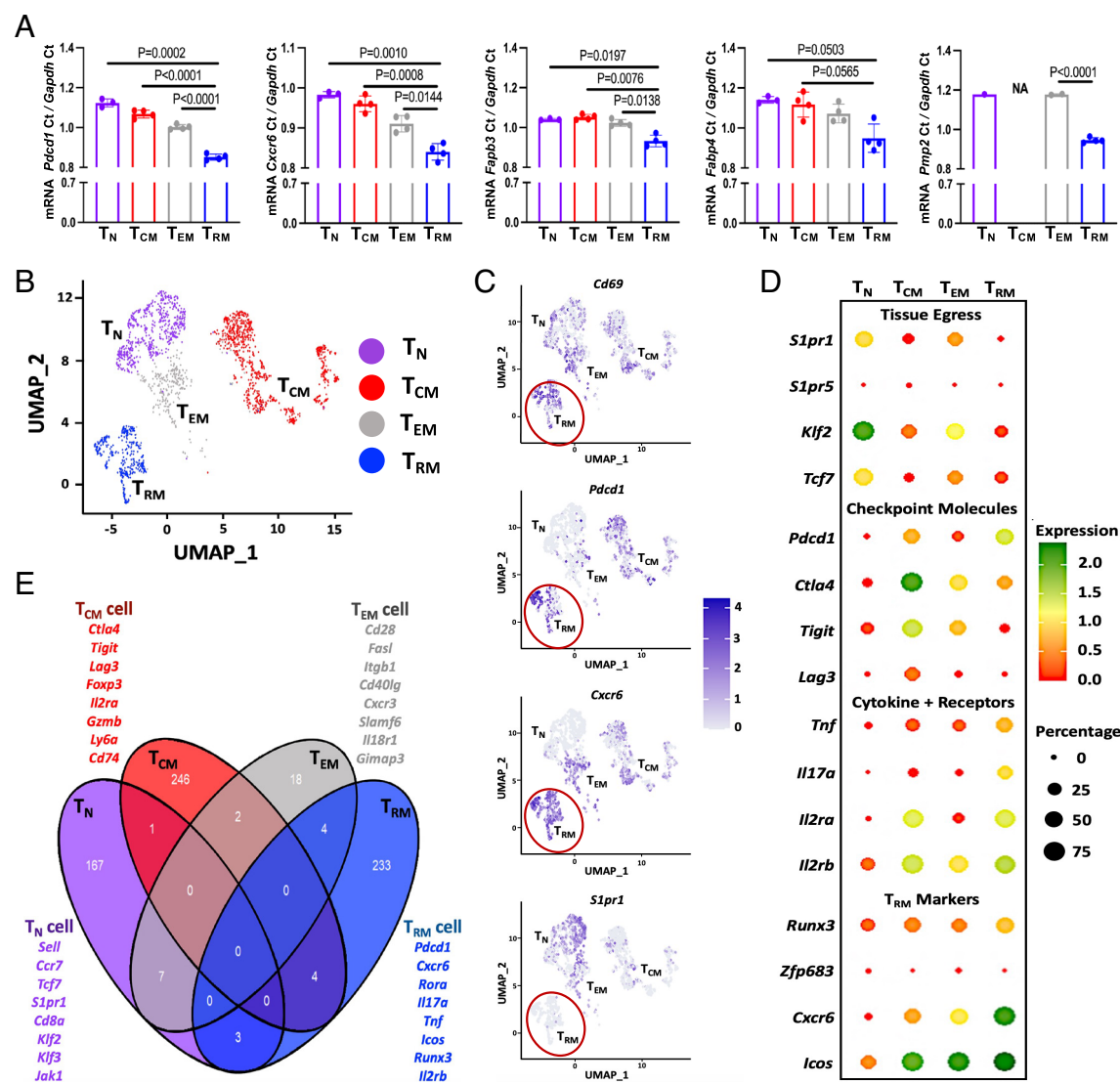


Fig. 2. Cardiac CD69⁺ T_{RM} cells are transcriptionally distinct from circulating T cells. (A) Peripheral and resident cardiac T cells were isolated from naive A/J mice and FACS sorted into distinct T_N, T_{CM}, T_{EM}, and T_{RM} cell populations. Graphs depict the Ct values as a ratio over the housekeeping gene *Gapdh*, meaning that lower ratios depict higher expression levels. n = 3 or 4 with each n representing 4 to 5 mice that were pooled together. Aged (46 wk) retired male and female breeders were used for pooling. Statistical significance was determined through a one-way Brown–Forsythe and Welch ANOVA. A t test was used to determine the significance of *Pmp2* expression. (B) Uniform Manifold Approximation and Projection (UMAP) clustering of cardiac T cells. (C) Feature plots showing gene expression of *Cd69*, *Pdcd1*, *Cxcr6*, and *S1pr1* in the various T cell clusters. (D) Bubble plot showing genes differentially expressed by distinct cardiac T cell populations. Statistical significance was assessed by a Wilcoxon signed-rank test. (E) Graphical depiction of the significantly up-regulated genes by each cardiac T cell subcluster.

trending increase in CD4⁺ T_{RM} cells but not CD8⁺ T_{RM} cells (Fig. 3*F* and *SI Appendix*, Fig. S3*D*). To investigate the phenotype of the recruited MyHC T_{RM} cells, we induced mEAM and allowed mice to recover for 8 wk before staining for FoxP3 and CD25. Similar to our findings in naive A/J mice (Fig. 1 *H* and *I*), we found that a majority of induced MyHC T_{RM} cells were Tconv cells and not Tregs (*SI Appendix*, Fig. S3*E*). To determine whether other models of cardiac injury would lead to the induction of CD69⁺PD-1⁺ T_{RM} cells, we employed an ischemia–reperfusion (I/R) mouse model, where ischemia was induced for 60 min followed by a 7-wk recovery period (Fig. 3*G*). We found that mice who recovered from I/R injury had no difference in the number of CD69⁺PD-1⁺CD4⁺ T_{RM} cells compared to mice who received sham surgery but had a significant increase in CD69⁺PD-1⁺CD8⁺ T_{RM} cells (Fig. 3*H* and *SI Appendix*, Fig. S3*F*). This indicates that the type of cardiac injury may influence whether CD4⁺ or CD8⁺ T cells are recruited to the heart and eventually mature into cardiac T_{RM} cells. It has been shown that T_{RM} cells accumulate in the peripheral organs, such as the skin, during aging

(46, 47). To determine the effect of aging on the recruitment of T_{RM} cells into the heart, we performed intravascular labeling on young (15 wk) and aged (53 wk) naive A/J mice. We found that aged mice had a significant increase in CD8⁺ T_{RM} cells but not CD4⁺ T_{RM} cells compared to young A/J mice (Fig. 3*I* and *SI Appendix*, Fig. S3*G*). Collectively, we determined that cardiac injury and aging lead to the accumulation of CD69⁺ PD-1⁺ T_{RM} cells in the heart.

Cardiac Injury Causes Accumulation of T_{RM} Cells Along the Perimyocardium. To determine the location of CD69⁺ T_{RM} cells in the heart, we utilized the mEAM mouse model to induce CD69⁺ PD-1⁺ T_{RM} cells (Fig. 3*A*). After induction of the disease, we allowed mice to recover for 8 wk before assessing residual inflammation via histology. We observed that 40% of the mice that received mEAM developed modest perimyocarditis, especially around the right ventricle (Fig. 4*A*). We found no observable infiltration in other areas of the heart, such as the atria and the ventricular myocardium (Fig. 4*A*). To identify the location of

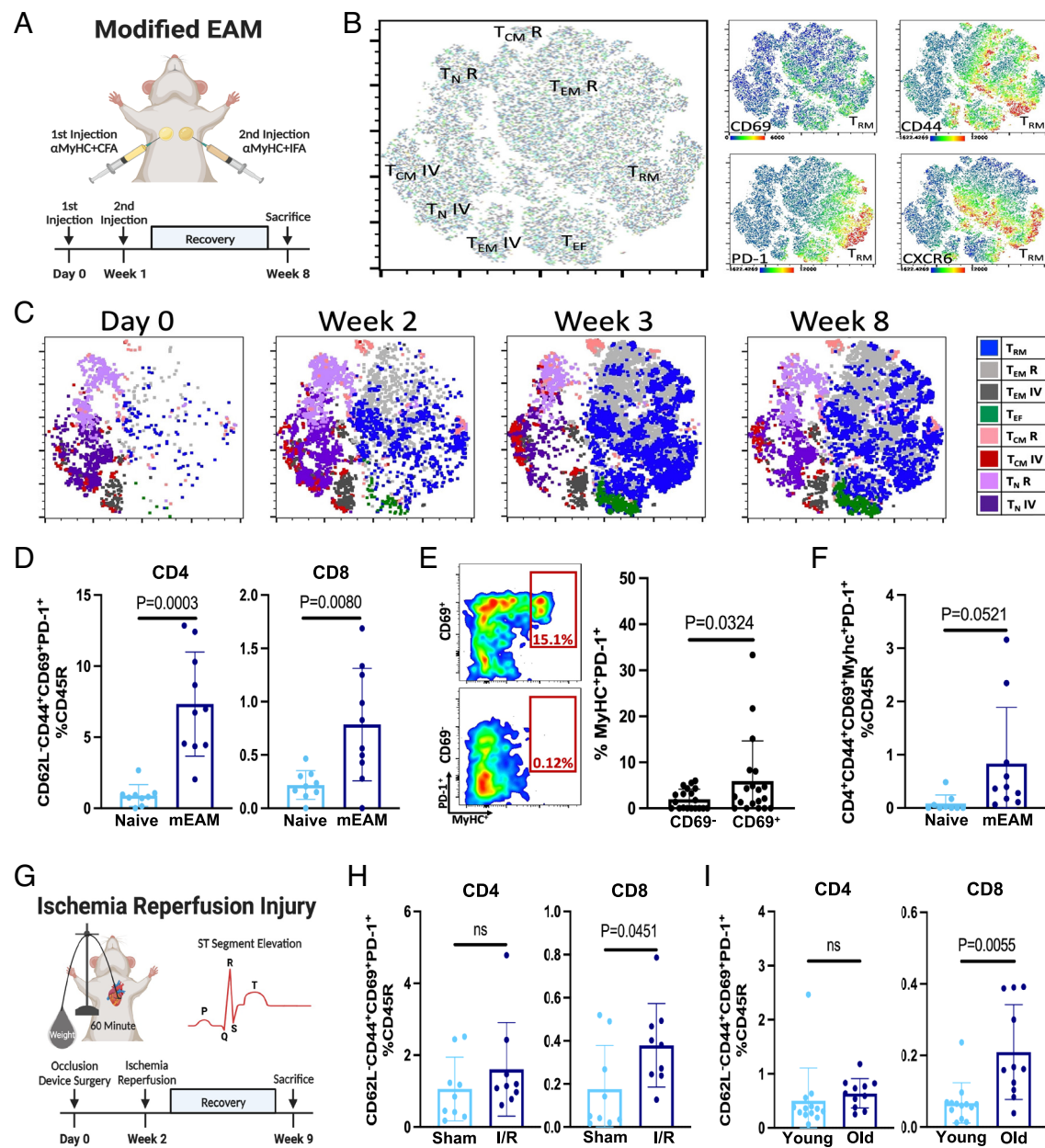


Fig. 3. Cardiac injury induces autoreactive cardiac CD69⁺PD-1⁺ T_{RM} cells. (A) Graphical description of mEAM mouse model timeline. (B) A/J mice from all groups were concatenated into a single file before unsupervised t-SNE clustering was performed on the cardiac CD4⁺ T cells. T-SNE clusters were assigned conventional T cell populations based on the expression of CD62L, CD44, KLRG1, and CD69. Infiltrating T cells (CD45IV) and resident immune T cells (CD45R) were labeled. Heat map illustrating the expression of the core T_{RM} cell genes CD69, CD44, PD-1, and CXCR6. The experiment has a total of n = 12. (C) Time course of mEAM showing the distribution of CD4⁺ T cells on weeks 0, 2, 3, and 8. (D) mEAM was induced in A/J mice, and after 8 wk, the number of T_{RM} cells was assessed by flow cytometry. Quantifying the proportion of CD4⁺ and CD8⁺ T_{RM} cells after mEAM compared to naive A/J mice. Group size was n = 9 or 10 mice. Statistical significance was determined through a Welch t test. (E) Representative flow graph showing expression of PD-1 and TCR specificity for cardiac myosin on resident CD69⁻ and CD69⁺ CD4⁺ T cells. Both naive mice and mEAM mice were included in this analysis. Group size was n = 19. Statistical significance was determined through a paired t test. (F) Graph quantifying the proportion of autoreactive myosin-specific CD69⁺PD-1⁺CD4⁺ T_{RM} cells after mEAM. Group size was n = 9 or 10 mice. Statistical significance was determined through a Welch t test. (G) Graphical description of I/R mouse model timeline. (H) I/R injury was induced in male A/J mice; after 8 wk, the number of T_{RM} cells was assessed by flow cytometry. Quantifying the proportion of CD4⁺ and CD8⁺ T_{RM} cells after I/R injury compared to A/J mice who received sham surgery. Group size was n = 9. Statistical significance was determined through a Welch t test. (I) Quantifying the proportion of CD4⁺ and CD8⁺ T_{RM} cells in young mice (15 wk) to aged mice (53 wk). Group size was n = 13 or 11. Statistical significance was determined through a Welch t test.

T cells in the heart, we performed immunohistochemistry (IHC) and stained for CD3. We found that mEAM induced accumulation of T cells predominantly along the perimyocardium but also in the atria (Fig. 4B). To confirm that these T cells were cardiac T_{RM} cells, we performed IHC for PD-1, Runx3, and CXCR6 and found that a majority of the cells along the atria and the perimyocardium were stained for all the T_{RM} cell markers (Fig. 4C). Thus, we determined that cardiac injury induces the accumulation of cardiac T_{RM} cells within the atria and along the ventricular perimyocardium.

Previous Cardiac Injury Increases the Susceptibility of Mice to Develop ICI-Myocarditis. ICI-myocarditis is a rare but fatal adverse event caused by treatment with antibodies binding to PD-1 or PD-L1 (7, 9). We show that cardiac injury induces autoreactive MyHC T_{RM} cells that express high levels of PD-1 (Fig. 3 E and F). These findings led us to hypothesize that autoreactive MyHC T_{RM} cells are susceptible to activation by αPD-1 antibodies and go on to mediate ICI-myocarditis. To test this hypothesis, we developed a double-hit ICI-myocarditis mouse model (Fig. 5A). In this model, we first induce

autoreactive MyHCT_{RM} cells through mEAM and then allow mice to recover for 8 wk to resolve cardiac inflammation before starting treatment with αPD-1 antibodies (Fig. 5A). To assess the severity of myocarditis, we evaluated heart tissue samples stained with H&E and found that mice who received mEAM + αPD-1 antibodies had a higher severity of cardiac inflammation compared to mice treated with αPD-1 antibodies alone (Fig. 5B and C). Next, we assessed the incidence of atrial and ventricular myocarditis separately. We found that mice who received mEAM + αPD-1 antibodies had an atrial myocarditis incidence rate of 62.5% compared to 20% in the control groups (Fig. 5D). When assessing the incidence of ventricular myocarditis, we found that mice who received mEAM + αPD-1 antibodies had an incidence rate of 67.3% (Fig. 5D). In comparison, none of the mice who received αPD-1 antibodies alone went on to develop ventricular myocarditis, while 50% of the mice who received mEAM+Isotype antibodies had low levels of remaining ventricular myocarditis (Fig. 5D). Next, we characterized the immune profile of cardiac inflammation by flow cytometry. We found that mice who received mEAM + αPD-1 antibodies had a trending increase in cardiac leukocytes, NK cells, and γδT cells (Fig. 5E and *SI Appendix*, Fig. S4A). Our lab and others have shown that the disease pathogenesis of ICI-myocarditis is driven by CD8⁺ T cells (11, 12). We found that mice who received mEAM followed by αPD-1 antibodies had a significant increase in CD3⁺ T cells, specifically CD8⁺ T cells (Fig. 5F and G and *SI Appendix*, Fig. S4B). To investigate whether other types of cardiac injury could increase susceptibility to ICI-myocarditis development, we induced the recruitment of T_{RM} cells through our I/R mouse model before starting αPD-1 antibodies (Fig. 5H). We then assessed the severity of cardiac inflammation through histology and found that mice receiving I/R + αPD-1 antibodies had increased immune infiltration compared to those receiving αPD-1 alone (Fig. 5I). Next, we assessed the incidence of ICI-myocarditis. To do this, we separately examined the atria and nonischemic regions of the ventricular myocardium. We found that mice receiving I/R + αPD-1 antibodies had a higher incidence of atrial myocarditis compared to control groups (Fig. 5J). Finally, we assessed ventricular myocarditis; to do this, we scored the incidence of myocarditis outside the zone of infarction. We found that mice who received I/R + αPD-1 antibodies had a myocarditis incidence of 41.7%. In contrast, mice who received sham surgery followed by αPD-1 antibodies had an incidence rate of 25%, while mice who received I/R+ Isotype antibodies had an incidence rate of 18.2% (Fig. 5J). Our findings indicate that previous cardiac injury induces autoreactive PD-1⁺ T_{RM} cells in the heart, which

increases the susceptibility of mice to develop ICI-myocarditis after PD-1/PD-L1 blockade.

Human Pericardial Fluid Is Enriched with CD69⁺PD-1⁺ T_{RM} Cells. Like mice, human cardiac T_{RM} cells have yet to be characterized. Our investigation of murine cardiac T_{RM} cells has demonstrated that cardiac injury leads to the recruitment of CD69⁺PD-1⁺ MyHCT_{RM} cells (Fig. 3F), defined by their location along the perimyocardium (Fig. 4B and C). To test whether chronic cardiac inflammation leads to the accumulation of human T_{RM} cells in the pericardial cavity, we examined blood and pericardial fluid samples from patients with ischemic cardiomyopathy (iCMP) and with dilated cardiomyopathy (DCM), where genetic causes were not identified. We chose to research DCM patients since one-third of patients diagnosed with myocarditis develop DCM (42, 48, 49). The development of ischemic cardiomyopathy (iCMP) is a chronic condition caused by ischemic injury and accompanying cardiac inflammation (50). Thus, DCM and iCMP are similar to the two types of cardiac injury we investigated with our murine models. We received pericardial fluid and blood samples from patients undergoing cardiac catheterization at the Institute of Clinical and Experimental Medicine (IKEM) in the Czech Republic (Fig. 6A and *SI Appendix*, Table S2). First, we assessed the distribution of CD4⁺ and CD8⁺ T cells in the pericardial fluid and PBMCs and found no difference in the CD4⁺:CD8⁺ ratio based on T cell location or disease diagnosis (*SI Appendix*, Fig. S5A and B). To assess the phenotype of pericardial T cells, we performed unbiased clustering through t-SNE and assigned T cell subsets based on conventional markers such as CD45RA, CCR7, and CD69 (*SI Appendix*, Fig. S5C). We found that CD4⁺ T cells subclustered into distinct biologically relevant populations and that pericardial T_{RM} cells grouped separately from the other T cell subtypes (Fig. 6B). We determined that T_{RM} cells were absent in PBMCs but were the predominant population in pericardial fluid (Fig. 6B). Next, we analyzed the expression of CD69 and PD-1 and found that they were predominately expressed by pericardial T_{RM} cells compared to circulating T cells (Fig. 6B–D). Similar to our previous finding (*SI Appendix*, Fig. S5B), we determined that the patient's cardiovascular diagnosis did not affect the proportion of CD69⁺ T_{RM} cells in pericardial fluid (*SI Appendix*, Fig. S5D). We found that both DCM and iCMP patients had on average, greater than 80% of their CCR7⁺CD45RA⁺ T cells expressing CD69 in both CD4⁺ and CD8⁺ T cells (*SI Appendix*, Fig. S5D). We showed that murine T_{RM} cells up-regulated PD-1 compared to other cardiac T cell populations (Figs. 1E and 2D), therefore, we assessed the expression of PD-1 on human pericardial T cells and found that, on average,

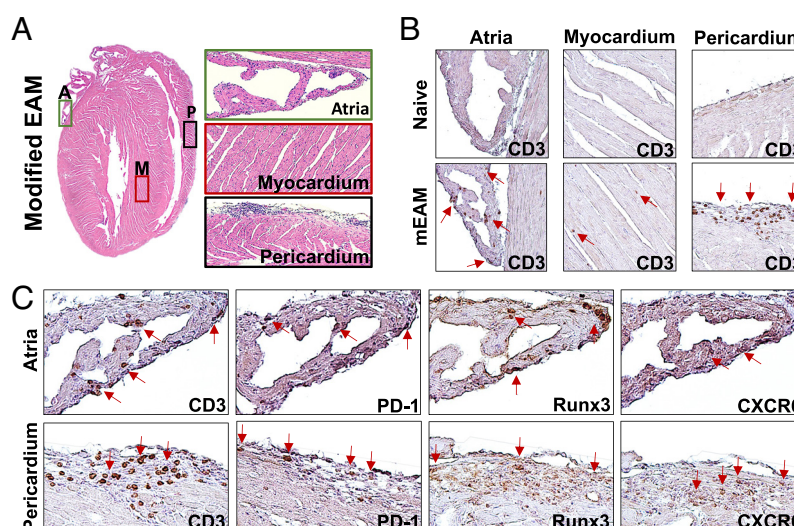


Fig. 4. Cardiac injury causes accumulation of T_{RM} cells along the perimyocardium. (A) Representative H&E histology of a mouse heart induced with mEAM. (B) Immunohistochemistry (IHC) showing the distribution of CD3⁺ T cells on representative histology of murine atria, myocardium, and pericardium in naive mice or mice who have recovered from mEAM. (C) IHC showing staining of CD3, PD-1, Runx3, and CXCR6 on representative histology from mice who recovered from mEAM.

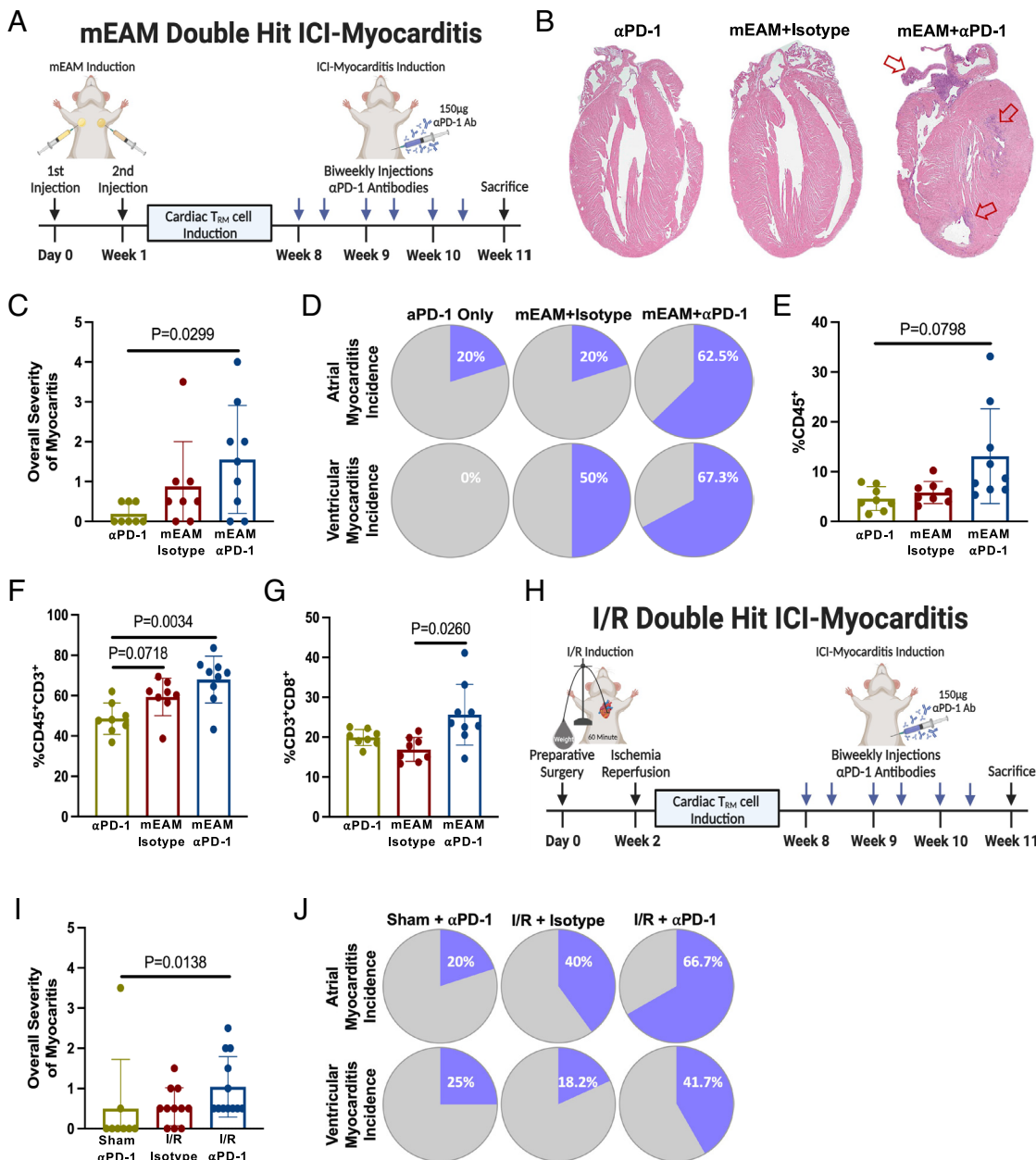


Fig. 5. Previous cardiac injury increases the susceptibility of mice to develop ICI-myocarditis. (A) Graphical description of ICI-myocarditis mouse model where cardiac T_{RM} cells were induced in A/J mice through mEAM. (B) Representative H&E histology of mice hearts, where mice received αPD-1, EAM+isotype, or EAM + αPD-1. (C) Histological assessment was used to determine the severity of myocarditis in mice. Group size was n = 8 or 9. Statistical significance was determined by the Kruskal-Wallis test. (D) Pie charts showing the incidence of atrial and ventricular myocarditis between. (E-G) Bar graphs showing the proportion of cardiac leukocytes, CD3⁺ T cells, and CD8⁺ T cells as determined by flow cytometry. Group size was n = 8 or 9. Statistical significance was determined by the Brown-Forsythe and Welch ANOVA test. (H) Graphical description of ICI-myocarditis mouse model where cardiac T_{RM} cells are induced by I/R injury in male A/J mice. (I) Histological assessment was used to determine the severity of myocarditis in mice. Group size was n = 9, 11, or 12. Statistical significance was determined by the Kruskal-Wallis test. (J) Pie charts showing the incidence of atrial and ventricular myocarditis.

74% of CD4⁺ pericardial T_{RM} cells expressed PD-1, compared to only 11% of T_N cells, 38% of T_{CM} cells and 47% of T_{EM} cells (Fig. 6 E and F). When accessing the expression of PD-1 on pericardial CD8⁺ T_{RM} cells, we found that, on average, 91% of CD8⁺ T_{RM} cells expressed PD-1, which was higher when compared to other CD8⁺ pericardial T cell populations (Fig. 6F). Next, we investigated the cytokine profile of DCM and iCMP patient pericardial fluid through a 48-cytokine multiplex (Millipore Sigma). We investigated the concentration of IL-2, IL-10, IL-15, TNF, IFN-γ, IL-17A, and IL-17F and found that only IL-10 and IL-15 were up-regulated in pericardial fluid (Fig. 6G and *SI Appendix*, Fig. S5E). IL-15 is necessary for the maintenance of T_{RM} cells in the kidney and skin (23, 44), thus, the presence of IL-15 may be required for pericardial T_{RM} cell survival. We ran a linear regression analysis and found that the concentration of pericardial IL-15 positively correlated with the number of pericardial T cells (Fig. 6H). IL-15 is produced by a variety of nonhemopoietic and hemopoietic cells, including epithelial cells, dendritic cells, and macrophages (51–53). It has

been shown that resident myeloid cells can support T_{RM} cell survival in the peripheral tissues through local production of chemokines and cytokines (22, 44). The pericardial cavity is known to be a reservoir for resident cardiac GATA6⁺ macrophages (54–56), which may be supporting resident T_{RM} cell population through the local production of IL-15 and IL-10. To assess the source of pericardial IL-15 and IL-10, we performed single-nucleus RNA sequencing on pericardial cells from patients diagnosed with iCMP (57). We then evaluated the gene transcript for both IL-15 and IL-10 and found that they were up-regulated by pericardial macrophages compared to pericardial NK and T cells (Fig. 6I). Therefore, pericardial IL-15 and IL-10 are most likely secreted by pericardial macrophages. Together, these findings demonstrate that DCM and iCMP patients have pericardial T_{RM} cells that express CD69 and PD-1, which are supported by pericardial macrophages through the production of IL-15. Collectively, our findings indicate that human and murine cardiac T_{RM} cells can be found in the pericardial cavity and share a similar CD69⁺PD-1⁺ phenotype.

Discussion

T_{RM} cells are noncirculating lymphocytes that coordinate rapid effector functions upon stimulation (14, 15, 25). T_{RM} cells are phenotypically and transcriptionally distinct cell types, which can be identified through classical markers such as CD69 and CD103 (14, 15, 17). We first set out to characterize T_{RM} cells in the hearts of naive mice. Compared to circulating lymphocytes, we found that cardiac memory T cells up-regulated CD69 but not CD103. CD69 has also been shown to distinguish resident memory T cells across various peripheral tissues and is expressed by T_{RM} cells in barrier organs such as the skin and nonbarrier organs such as the salivary gland, pancreas, and liver (17, 22, 28, 30, 44). CD69 is an important marker for defining T_{RM} cells since it facilitates tissue retention by antagonizing egress proteins (18, 19). CD103 is an integrin that binds E-cadherin and is predominately expressed by T_{RM} cells in epithelial tissues such as the lung and the skin (58–60). To further characterize cardiac T_{RM} cells, we transcriptionally profiled cardiac T cells from naive mice and mice who received EAM. We found that cardiac T_{RM} cells up-regulated the crucial transcription factor Runx3, which is important for the upregulation of tissue retention genes in both murine and human T_{RM} cells (40, 41). Transcriptional reprogramming by Runx3 is important for T_{RM} cell recruitment and maintenance in various tissues, such as the intestines and lungs (40, 41). Transcriptional reprogramming of memory T_{RM} cells is associated with altered metabolism, specifically the upregulation of fatty acid oxidation (37, 38). Furthermore, T_{RM} cells have been shown to up-regulate tissue-specific isoforms of the FABPs, which facilitate the uptake of lipids by resident immune cells (37, 38). We found the cardiac CD69⁺ T_{RM} cells up-regulated three of the nine FABP isoforms, FAPB3, FAPB4, and Pmp2. Upregulation of specific FABP isoforms has been shown to be crucial for T_{RM} cell function and survival in the peripheral tissues; for example, FAPB4 and FAPB5 are important for skin T_{RM} cells, while FAPB1 is necessary for liver T_{RM} cells (37, 38). Thus, we were able to conclusively demonstrate that cardiac T_{RM} cells are present in naive mice and can be distinguished from circulating T cells by their expression of the classical T_{RM} marker CD69, the transcription factor Runx3, and the metabolic proteins FAPB3, FAPB4, and Pmp2.

To further characterize cardiac T_{RM} cells, we used a comprehensive approach that included transcriptional profiling and intravascular labeling to determine the residency of CD69⁺ cardiac T_{RM} cells. To determine whether cardiac T_{RM} cells featured transcriptional changes that would support residency in the peripheral tissues, we profiled cardiac T cells from naive mice and mice who received EAM. We found cardiac T_{RM} cells down-regulated the tissue egress protein S1PR1 and the transcription factor KLF2. Vertebrate animals contain five distinct receptors for S1P, which aid in embryogenesis, cell signaling, and lymphocyte egress (19, 61, 62). Downregulation of S1PR1 is necessary for the formation and maintenance of both human and murine T_{RM} cells (17, 18). KLF2 is a zinc finger transcription factor that stimulates lymphocyte egress by promoting the transcription of S1PR1 (63). Downregulation of KLF2 promotes T_{RM} formation within peripheral tissues and has been documented in a variety of organs, such as the kidney, brain, and salivary gland (14). To further investigate the residency of cardiac CD69⁺ T_{RM} cells, we employed IV labeling to distinguish cells trapped within the vasculature and those occupying the tissue. We confirmed that the expression of CD69 was exclusive to resident T cells compared to lymphocytes trapped within the cardiac vasculature. It has been shown that the perfusion of organs after killing of animals is insufficient to remove circulating immune cells, which can confound the identification and characterization of resident leukocytes (35). Intravascular labeling is an effective method to discriminate the location and residency of

murine T_{RM} cells in peripheral tissues such as the lung, kidney, and skin (31, 35, 64). Therefore, we were able to demonstrate, through transcriptional analysis and intravascular labeling, that cardiac CD69⁺ T cells are conclusively resident memory T cells.

Autoimmune MyHCT cells escape negative selection in the thymus and can be found in the periphery of naive mice and humans (32). Our previous studies have characterized MyHCT cells in naive murine hearts and found that they demonstrate an antigen-experienced phenotype as well as up-regulate CD69 (11). To determine whether MyHCT cells are cardiac resident, we combined intravascular labeling with tetramer staining. We found that a significant proportion of MyHCT cells were cardiac resident and up-regulated CD69. Autoimmune T cells have been identified within healthy-appearing tissues and have been proven to exhibit a T_{RM} -like signature (15, 65). Furthermore, T_{RM} cells have been implicated in various autoimmune diseases such as vitiligo and psoriasis (15, 28, 65). During inflammation, activated T cells are primed in the secondary lymphoid organs before being recruited into the peripheral tissues (66, 67). After the resolution of inflammation, there is a significant contraction, and a small population of mature T_{RM} cells remain (66, 67). In the heart, it has been shown that MyHCTregs are recruited during the acute phase of ischemic injury and play a protective role during cardiac remodeling (33, 34). To determine how myocardial damage would affect the autoimmune MyHCT T_{RM} cells population, we employed the mEAM and I/R injury mouse models to induce cardiac damage. We found that cardiac injury induced an increase in autoimmune CD69⁺ MyHCT T_{RM} cells. Phenotyping of these T_{RM} cells demonstrated that they appear predominantly to be conventional T cells and not Tregs. However, due to the limitations of flow cytometry in stratifying rare populations, we can't exclude the possibility that some MyHCT T_{RM} cells are Tregs. Recruitment of antigen-specific T_{RM} cells has been documented in a variety of murine tissues following an infection, vaccination, or injury (22, 23, 31, 64). It has been demonstrated that antigen-specific T_{RM} cells maintain rapid effector function upon restimulation, which can be protective against subsequent viral challenges or pathogenic in the case of allergen-induced asthma (22, 68). Aging is associated with reduced thymopoiesis and increased recruitment of T_{RM} cells into the peripheral tissues (46). To determine the effect of aging on MyHCT T_{RM} cells, we performed intravascular labeling on naive young and aged mice. We found that aged mice had an increased proportion of CD8⁺CD69⁺ T_{RM} cells. It has been shown that aged mice accumulate CD8⁺ T_{RM} cells in the lung, which induces chronic inflammation, leading to tissue fibrosis (69). In addition, aging is associated with a reduction of cardiac function, which has been linked to T cell accumulation in the mediastinal lymph nodes (70, 71). Overall, we were able to establish that MyHCT cells are cardiac T_{RM} cells, which expand after cardiac injury and accumulate in the heart during aging.

T_{RM} cells are highly activated resident immune cells that up-regulate PD-1 in a variety of tissues, such as the lung, skin, and pancreas (14, 30, 31). It has been shown that the PD-1/PD-L1 axis is a critical negative regulator of T_{RM} cells, which helps maintain immune homeostasis and prevents tissue fibrosis (30, 31). To further characterize MyHCT T_{RM} cells, we examined the expression of PD-1 and found that MyHCT cells significantly up-regulated both CD69 and PD-1. Although PD-1 expression is typically associated with loss of effector function, a hallmark of T cell exhaustion, T_{RM} cells maintain effector polyfunctionality despite high levels of PD-1 expression (30, 31). ICI-myocarditis is a highly fatal irAE, which occurs rapidly after beginning immune checkpoint blocking therapies and predominantly affects patients treated with immunotherapies targeting the PD-1/PD-L1 axis (7, 8). The majority of patients develop ICI-myocarditis after only 1 to 2 treatments with a median onset time of 34 d (7, 9, 10, 72). The rapid development of the disease indicates

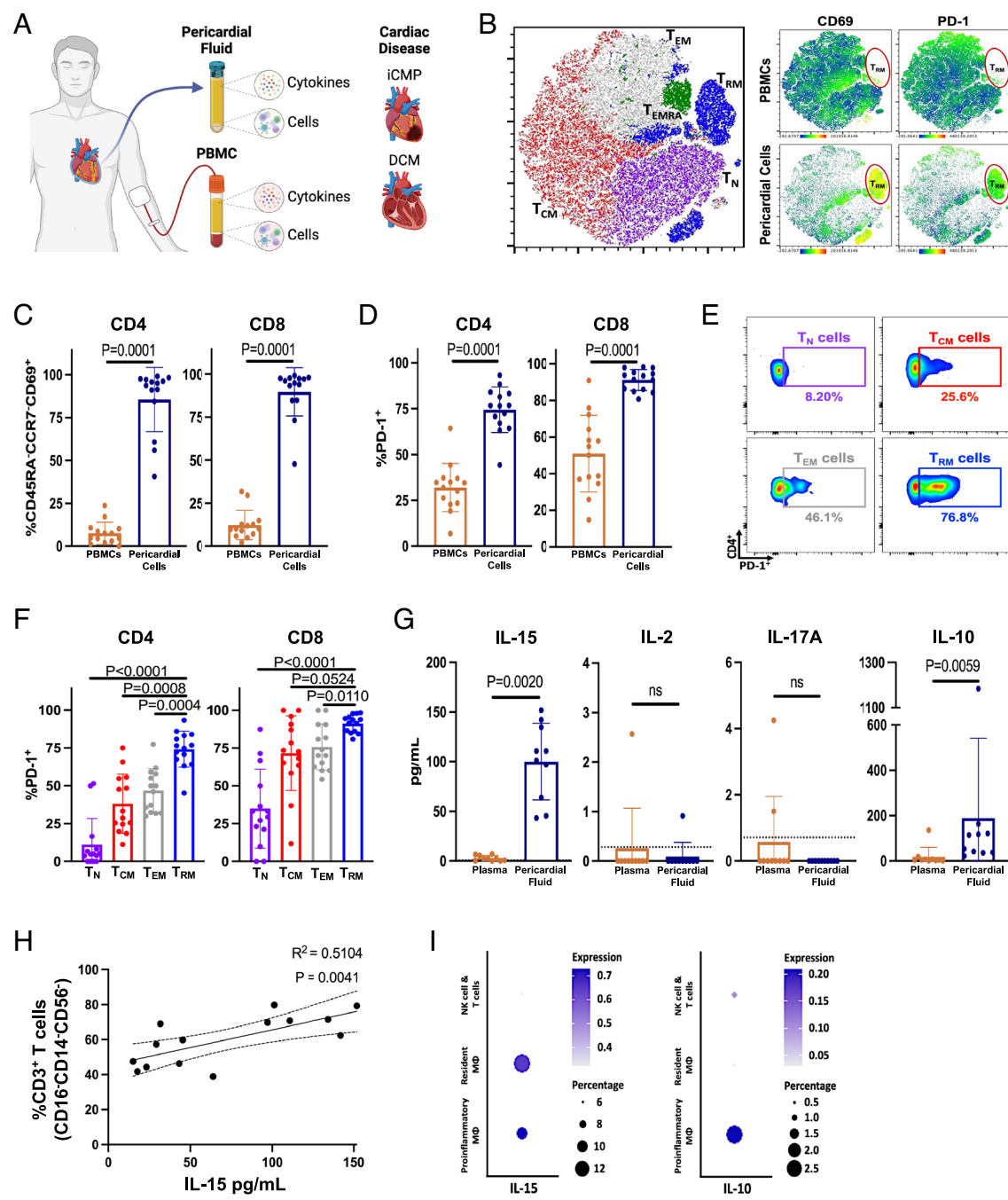


Fig. 6. Human pericardial fluid is enriched with CD69⁺PD-1⁺ T_{RM} cells. (A) Graphical depiction of deidentified human patient samples received from the biorepository at the Institute for Clinical and Experimental Medicine (IKEM). Samples were collected from patients diagnosed with either dilated cardiomyopathy (DCM) or ischemic cardiomyopathy (iCMP). (B) Patient PBMCs and pericardial cells concatenated into a single file before unsupervised t-SNE clustering was performed on the CD4⁺ T cells. Heat mapping illustrating CD69 and PD-1 expression on CD4⁺ T cells from patient PBMCs and pericardial cells. (C and D) Expression of CD69 and PD-1 on CD4⁺ and CD8⁺ T cells on patient PBMCs and pericardial cells. Group size was $n = 14$. Statistical significance was determined by the Wilcoxon test. (E) Representative flow plots showing the expression of PD-1 on T_N, T_{CM}, T_{EM}, and T_{RM} pericardial CD4⁺ T cells. Group size was $n = 14$. Statistical significance was determined by the RM one-way ANOVA. (F) Expression of PD-1 on different pericardial T cell populations. Group size was $n = 14$. Statistical significance was determined by the Wilcoxon test. (G) Comparing the concentrations of cytokines in human pericardial fluid compared to matched patient plasma. Group size was $n = 10$. Statistical significance was determined by the Wilcoxon test. (H) Simple linear regression analysis comparing the pericardial fluid concentration of IL-15 to the proportion of CD3⁺ T cells (from lineage⁻ gate). Group size was $n = 14$. (I) Bubble plot showing gene expression of IL-15 and IL-10 by pericardial macrophages and NK and T cells.

that certain patients may be predisposed to develop ICI-myocarditis. Risk factors for ICI-myocarditis development include the combination of ICI therapies, age, previous cardiovascular disease, and diagnosis of an autoimmune disease (7, 72). To determine whether resident autoimmune CD69⁺ MyHC T_{RM} cells are responsible for ICI-myocarditis, we created mouse models where we induced MyHC T_{RM} cells either through mEAM or I/R injury and started treatment with αPD-1 antibodies after recovery from these cardiac injuries. We determined that mice with more CD69⁺ MyHC T_{RM} cells had a

greater incidence of ICI-myocarditis development, as well as significant infiltration of CD8⁺ T cells. T_{RM}-like TILs have been described across various cancers and have been shown to highly up-regulate PD-1 as well as other immune checkpoint molecules (73, 74). Treatment with immune checkpoint therapies directly activate and expand T_{RM}-like TILs, which is clinically beneficial and is associated with a robust antitumor response in certain cancers like melanoma (73, 74). Thus, we demonstrated that ICI-myocarditis is mediated by MyHC T_{RM} cells that are enriched in the heart after cardiac injury.

Resident cardiac macrophages have been shown to be distributed throughout the heart (70, 75). In certain incidences, the cellular location has been linked to a specific function; for example, cardiac macrophages cluster around the atrioventricular bundle and provide support for electrical conduction (76). We determined that injury-induced cardiac T_{RM} cells were preferentially located within the atria and along the perimyocardium. To investigate the location of human cardiac T_{RM} cells, we received pericardial fluid samples from a biorepository at the Institute for Clinical and Experimental Medicine (IKEM) in the Czech Republic. For our study, we included patients diagnosed with dilated cardiomyopathy (DCM) and ischemic cardiomyopathy (iCMP). DCM is characterized by the dilation of the left ventricle, which causes impaired ventricular contraction and leads to reduced cardiac output (77, 78). Approximately one-third of patients diagnosed with myocarditis go on to develop DCM (77–79). iCMP is a chronic condition initiated through myocardial damage caused by ischemia, leading to impaired cardiac function (50, 80). We found that a majority of pericardial T cells express a resident memory phenotype and up-regulate CD69 and PD-1. In humans, it is known that T cells are key components of the inflammatory milieu recruited to the heart during myocardial inflammation (43, 81, 82). In mice, we found that cardiac injury induces autoreactive MyHC CD69⁺PD-1⁺ T_{RM} cells that preferentially locate along the perimyocardium. We determined CD69⁺PD-1⁺ T_{RM} cells are the predominant T cell population in the pericardial cavity in patients diagnosed with DCM and iCMP, which supports our finding that cardiac injury induced by mEAM and I/R injury induces autoreactive MyHC CD69⁺PD-1⁺ T_{RM} cells in mice. Our findings indicate that regardless of disease etiology, myocardial inflammation leads to the recruitment of pericardial PD-1⁺ T_{RM} cells. Finally, we determined that human T_{RM} cells have the highest expression of PD-1 compared to other pericardial T cell populations. Our finding that a majority of pericardial T_{RM} cells express PD-1 parallels our investigation of murine cardiac T_{RM} cells and suggests that human pericardial T_{RM} cells may also be susceptible to activation by αPD-1 antibodies.

The pericardial cavity hosts a variety of different leukocytes, such as GATA6⁺ resident macrophages and B cells (54, 55). In mice, T_{RM} cells in the female genital tract have been shown to form lymphocyte clusters with resident macrophages. This has been determined to be important for T_{RM} cell retention since macrophages provide support through chemokine production (22). To determine whether the microenvironment of the pericardial cavity could support T_{RM} cells, we performed a multiplex on pericardial fluid and plasma isolated from human patients. We found that human pericardial fluid was enriched for IL-15, which shares the same common γ-chain receptor as IL-2 (83). In our reanalysis of the publicly available single-cell RNA sequencing dataset, we found that murine cardiac T_{RM} cells differentially up-regulated the gene expression of the IL-2 receptor β-chain, indicating that cardiac T_{RM} cells are dependent on IL-15 signaling. IL-15 has been shown to be necessary for T_{RM} survival and maintenance in a variety of tissues, such as the skin and kidney (23, 44, 53). To determine the source of human pericardial IL-15, we performed single-nucleus RNA sequencing on pericardial immune cells from iCMP patients and found that pericardial macrophages were the main source of IL-15. This indicates that resident pericardial macrophages may be supporting the survival of pericardial T_{RM} cells, which may explain why murine and human CD69⁺PD-1⁺ T_{RM} cells preferentially locate along the perimyocardium. Collectively, our findings indicate that human and murine cardiac T_{RM} cells share a prominent CD69⁺PD-1⁺ phenotype and reside in the same location within the heart.

In summary, we were able to determine that CD69 is differentially expressed by cardiac tissue resident memory T cells, which are phenotypically and transcriptionally distinct from circulating

lymphocytes. We confirmed that murine autoreactive MyHC T cells are present in naive mouse hearts and demonstrated that MyHC T cells express CD69 and are tissue resident memory T cells. It is poorly understood why MyHC T_{RM} cells are recruited to the heart and what function they play during immune homeostasis, which should be the focus of future studies. MyHC T_{RM} cells are highly activated cells that up-regulate PD-1 and are recruited to the heart after cardiac injury or during aging. We were able to show that cardiac T_{RM} cells can be found within the atria and along the ventricular perimyocardium. However, how T_{RM} cells localize to the pericardial membrane remains uncertain. Finally, we demonstrated with our double-hit ICI-myocarditis mouse models that mice with more MyHC T_{RM} cells developed ICI-myocarditis more frequently and acquired more severe disease. Finally, we demonstrate the high translatability of our characterization of murine T_{RM} cells because we found CD69⁺PD-1⁺ T_{RM} cells are the predominant T cell population in pericardial fluid isolated from patients with DCM or iCMP. This study provides evidence that ICI-myocarditis is directly mediated by autoreactive MyHC T_{RM} cells and provides a mechanism for why age and previous cardiac injury are risk factors for ICI-myocarditis development.

Materials and Methods

Study Design. This study aimed to describe cardiac resident memory T cells and their contribution to the disease pathogenesis of ICI-myocarditis. In this study, we assessed the impact of aging and cardiac injury on the recruitment and retention of cardiac T_{RM} cells. Cardiac injury was induced either through a modified experimental autoimmune myocarditis model or an ischemia-reperfusion injury model. A detailed description of the experimental design, sample size, and statistical test can be found in the figure legends. All experiments were repeated as independent experiments two to three times unless otherwise stated in the figure legend.

Mice. Wild-type A/J breeders (strain#000646) were purchased from the Jackson Laboratory. Mice included in studies were female unless otherwise stated. All animals were housed in specific pathogen-free conditions at a Johns Hopkins University animal facility. Experiments were conducted on animals 8 to 12 wk old unless otherwise stated in the figure legend. All animal experiments were conducted under protocols reviewed and approved by the Animal Care and Use Committee at Johns Hopkins University.

Cell Isolation and Flow Cytometry. Hearts were perfused through the aorta with PBS for 3 min before being removed and chopped into small pieces. Hearts were digested with Collagenase II and DNase I for 30 min at 37 °C on a shaker. Tissue was dissociated and placed through a 70 μm cell strainer. Cells were washed and transferred to a 96-well plate for staining. Cells were blocked with anti-CD16/32 and sera for 30 min at 4 °C. Cells were stained with primary antibodies at 4 °C for 30 min. Cells were fixed overnight with BD Cytofix before being acquired on an LSRII Fortessa flow cytometer (BD), and data were analyzed using FlowJo software (BD). Detailed instructions including heart tissue processing, tetramer staining, and intravascular labeling can be found in *SI Appendix, Supplemental Methods*, and a list of antibodies and concentrations can be found in *SI Appendix, Table S3*.

qRT-PCR. A detailed description of how cells were prepared and sorted can be found in *SI Appendix, Supplemental Methods*. RNA was extracted from sorted cells using TRIzol reagent (Life Technologies, Cat#15596018). RNA was normalized before cDNA was synthesized using iScript Reverse Transcript Supermix (Bio-Rad, Cat#1708841). Genes of interest were amplified using PowerUp SYBER Green Master Mix (ThermoFisher, Cat#10029284). The samples were run on a MyiQ2 thermal cycler (Bio-Rad). The data were analyzed by comparing the Ct value of the gene of interest to the Ct value of the housekeeping gene Gapdh. Primers used in the study can be found in *SI Appendix, Table S4*.

Murine Single-Cell RNA Sequencing Analysis. The publicly available experimental autoimmune myocarditis single-cell RNA sequencing dataset was retrieved using the accession code: GSE142564 (39). Cells from different days were

combined using the merge command. Following regularized negative binomial regression normalization, cells were clustered via UMAP nonlinear dimensional reduction to allow biological cluster annotation. Clusters identified to be T cells were isolated and subclustered. T_{EF} were identified but were excluded from subsequent differential gene analysis. A detailed description of our quality control and subsequent analysis can be found in *SI Appendix, Supplemental Methods*.

Human Pericardial Single-Nucleus Isolation, Library Generation, Sequencing, and Analysis. Frozen cells were thawed and washed with culture media. Cells were treated with DNase for 5 min on ice. Pericardial cells were incubated in a lysis buffer on ice for 10 min. Nuclei were washed with a wash buffer and spun down. Nuclei were resuspended in chilled nuclei buffer and stained with TotalSeq™-B anti-human Hashtag antibodies for 20 min on ice. A detailed description of lysis, wash, and nuclei buffers is available in *(SI Appendix, Table S5)*. 3' HT single-nucleus RNA sequencing with barcoded cell hashing was performed using the 10x Genomics platform. Data were analyzed using the Seurat (v4.3.0) workflow in R (v4.3.0). Cells with nFeature_RNA > 250, nFeature_RNA < 7,000, nCount_RNA < 80,000, and percent_mt < 27) were examined. Following QC, 9367 cells were retained. Cells were normalized using the SCTransform method and then reduced via PCA and UMAP. Cells were clustered and separated into biologically meaningful populations. Gene expression was visualized using DotPlot() using the log-normalized gene expression count matrix.

Modified Experimental Autoimmune Myocarditis (mEAM) Induction. To induce mEAM, A/J mice were immunized with two 100 µg doses of the heavy α -chain of cardiac myosin peptide (MyHC α _{334–352} DSAFDVLSFTAEEKAGVYK), which was purchased from GenScript. For the first immunization, the cardiac myosin peptide was emulsified in Complete Freud's Adjuvant (Sigma-Aldrich, Cat#F5881), which had been supplemented with 40 mg of heat-killed *Mycobacterium tuberculosis* (Difco, Cat#DF3114-33-8). During the first immunization, mice were also administered 500 ng of pertussis toxin (List Biological Laboratories, Cat#180) through an IP injection. For the second immunization, the cardiac myosin peptide was emulsified in Incomplete Freud's Adjuvant (Sigma-Aldrich, Cat#F5506). Immunizations with myosin peptide occurred on Day 0 and Day 7, and both immunizations were administered SC.

Ischemia–Reperfusion (I/R) Mouse Model. Ischemia–reperfusion injury was induced in a two-step manner as previously published (84). A detailed description of the procedure can be found in *SI Appendix, Supplemental Methods*. Mice were intubated and connected to a respirator (Mini Vent 845) and anesthetized with isoflurane. Hair over the chest cavity was removed, the chest opened, a lateral thoracotomy was performed, and the rib cage opened. Using an 8-0 monofilament suture, an occlusion device (PE-10 tubing) was placed at 2 mm from the auricle. The ribcage was then sutured closed, and the remaining string from the 8-0 suture was stored under the skin. Mice were allowed to recover for 2 wk between surgeries. Mice were anesthetized with Ketamine and further anesthetized with 1 to 3% isoflurane. The skin was opened, and the string attached to the occluding device was taped to a 5 g lead weight. The lead weight was then hung on a bearing, allowing compression of the left anterior descending artery for 60 min. Afterward, the weight was removed, and the skin was closed with an 8-0 suture.

Cardiac Histology Assessment. Cardiac H&E slides were evaluated for immune infiltration with the following criteria. Score 0, no inflammation; score 1, <10%; score 2, 10 to 30%; score 3, 30 to 50%; score 4, 50 to 90%; and score 5, >90%. The atria, ventricular myocardium, and pericardium were evaluated separately. Slides were scored independently by two blinded investigators.

Immunohistochemistry. Unstained slides were baked at 60 °C for 20 min. Slides were placed in Trilogy (Cell Marque, Cat#920P-06) and cooked in a pressure cooker for 20 min. Slides were cooled and rinsed in distilled water. Slides were incubated for 5 min with the dual endogenous enzyme block (Dako, Cat#S2003) followed by a 1-h incubation in the primary antibody. Slides were rinsed before being incubated with the 2° antibodies (Leica, Cat#PV6119 or Cat#PV6114) for 30 min. Slides were rinsed

before incubating in DAB chromogen (Vector Laboratories, Cat#SK-4100) for 4 min. Slides were rinsed before being counterstained with Hematoxylin 1 (ThermoFisher, Cat#72221). Slides were rinsed and then placed in the Bluing reagent (Epredia, Cat#6769001) for 1 min before a sequential dehydration in ethanol. Slides were mounted with OPTICMOUNT 1 (Mercedes Scientific, Cat#MER7720) and left to cure overnight. A detailed list of antibodies and concentrations can be found in *SI Appendix, Supplemental Methods*.

Two-Hit ICI-Myocarditis Induction. T_{RM} cells were recruited to the heart either through mEAM or I/R injury. After the cardiac injury, mice were allowed to recover, and inflammation was allowed to resolve before beginning immune checkpoint inhibitor blocking therapies. Mice were treated IP with 150 µg of either α PD-1 antibodies (BioXCell, Cat#BE0146) or isotype control antibodies (BioXCell, Cat#BE0089) as previously published (11). Mice were treated biweekly for three weeks.

Human Samples. We obtained human pericardial fluid samples and PBMC from a biorepository at the Institute of Clinical and Experimental Medicine (IKEM) in the Czech Republic. Samples were collected at the institute, deidentified, and shipped to our lab at Johns Hopkins University. Upon receipt, the frozen samples were stored at –80 °C. We determined the cytokine composition of patient plasma and pericardial fluid through a 48-cytokine Multiplex (Milipore, Cat#HCYTA-60 K-PX48).

Statistical Analysis

Statistical significance analysis was performed by GraphPad Prism 10 software. Data were analyzed using a variety of tests such as the paired *t* test, Welch *t* test, paired one-way ANOVA with Geisser-Greenhouse corrections, Wilcoxon signed-rank test, simple linear regression, Brown-Forsythe and Welch ANOVA, and Kruskal-Wallis test. The statistical test used for each experiment has been included in all the figure legends. Numerical *P* values were included in the figures or labeled as nonsignificant (ns). Data are presented as the mean ± SD, and symbols represent individual samples, unless otherwise stated.

Data, Materials, and Software Availability. Original single-nucleus data have been deposited in figshare (<https://figshare.com/s/a3c29c74f375c9ae6025>) (57). All study data are included in the article and/or *SI Appendix*.

ACKNOWLEDGMENTS. Cell sorting was performed at the Bloomberg Flow Cytometry. Cardiac myosin tetramers were provided by the NIH tetramer core facility. Flow samples were run at the SKCCC Flow Core. Graphics made with the assistance of BioRender.com. This work was supported by the National Institute of Health, National Heart, Lung, and Blood Institute R01HL118183 (PI: D.C.), R01HL136586 (PI: D.C.), and F31AR077406 (PI: D.H.), and H.K. was supported by 2T32AI007417-26 and 5T32AI007417-25. The American Heart Association grants 19TPA3491007 (PI: D.C.), 20TPA35490421 (PI: D.C.), and 23EIA1040103 (PI: D.C.). As well as the Global Autoimmune Institute, the Matthew Poyer MVP Memorial Myocarditis Research Fund, the Katherine E. Welsh Fellowship, the Delta Omega Scholarship award (H.K.), and the 2018 Rhett Lundy Memorial Research Fellowship from the Myocarditis Foundation (T.W.). V.M., I.J., and I.S. were supported by the National Institute for Research of Metabolic and Cardiovascular Diseases (Program EXCELES, ID Project No. LX22NPO5104)–Funded by the European Union–Next Generation EU.

Author affiliations: ^aW. Harry Feinstone Department of Molecular Microbiology and Immunology, Bloomberg School of Public Health, Johns Hopkins University, Baltimore, MD 21205; ^bDepartment of Pathology, School of Medicine, Johns Hopkins University, Baltimore, MD 21205; ^cDepartment of Cardiology, Institute for Clinical and Experimental Medicine, Prague 140 21, Czech Republic; ^dDepartment of Chemical and Biomolecular Engineering, Whiting School of Engineering, Johns Hopkins University, Baltimore, MD 21205; and ^eDepartment of Clinical and Transplant Immunology, Institute for Clinical and Experimental Medicine, Prague 140 21, Czech Republic

1. G.J. Freeman *et al.*, Engagement of the Pd-1 immunoinhibitory receptor by a novel B7 family member leads to negative regulation of lymphocyte activation. *J. Exp. Med.* **192**, 1027–1034 (2000).
2. C.A. Chambers, T.J. Sullivan, J.P. Allison, Lymphoproliferation in CTLA-4-deficient mice is mediated by costimulation-dependent activation of CD4+ T cells. *Immunity* **7**, 885–895 (1997).
3. H. Ueda *et al.*, Association of the T-cell regulatory gene CTLA4 with susceptibility to autoimmune disease. *Nature* **423**, 506–511 (2003).
4. H. Nishimura, N. Minato, T. Nakano, T. Honjo, Immunological studies on PD-1 deficient mice: Implication of PD-1 as a negative regulator for B cell responses. *Int. Immunol.* **10**, 1563–1572 (1998).

5. F. Martins *et al.*, Adverse effects of immune-checkpoint inhibitors: Epidemiology, management and surveillance. *Nat. Rev. Clin. Oncol.* **16**, 563–580 (2019).
6. S. Tan, D. Day, S. J. Nicholls, E. Segelov, Immune checkpoint inhibitor therapy in oncology: Current uses and future directions: JACC: Cardiology state-of-the-art review. *JACC CardioOncol.* **4**, 579–597 (2022).
7. D. Y. Wang *et al.*, Fatal Toxic Effects Associated With Immune Checkpoint Inhibitors. *JAMA Oncol.* **4**, 1721 (2018).
8. M. Dougan, A. M. Luoma, S. K. Dougan, K. W. Wucherpfennig, Understanding and treating the inflammatory adverse events of cancer immunotherapy. *Cell* **184**, 1575–1588 (2021).
9. J. J. Moslehi, J. E. Salem, J. A. Sosman, B. Lebrun-Vignes, D. B. Johnson, Increased reporting of fatal immune checkpoint inhibitor-associated myocarditis. *Lancet* **91**, 933 (2018).
10. N. Palaskas, J. Lopez-Matei, J. B. Durand, C. Iliescu, A. Deswal, Immune checkpoint inhibitor myocarditis: Pathophysiological characteristics, diagnosis, and treatment. *J. Am. Heart Assoc.* **9**, e013757 (2020).
11. T. Won *et al.*, Cardiac myosin-specific autoimmune T cells contribute to immune-checkpoint-inhibitor-associated myocarditis. *Cell Rep.* **41**, 111611 (2022).
12. M. L. Axelrod *et al.*, T cells specific for α -myosin drive immunotherapy-related myocarditis. *Nature* **611**, 818–826 (2022).
13. D. Cibrán, F. Sánchez-Madrid, CD69: from activation marker to metabolic gatekeeper. *Eur. J. Immunol.* **47**, 946–953 (2017).
14. P. A. Szabo, M. Miron, D. L. Farber, Location, location, location: Tissue resident memory T cells in mice and humans. *Sci. Immunol.* **4**, eaas9673 (2019).
15. S. C. Sisson, C. L. Gordon, S. N. Christo, P. Kleenerman, L. K. Mackay, Local heroes or villains: Tissue-resident memory T cells in human health and disease. *Cell Mol. Immunol.* **17**, 113–122 (2020).
16. D. Masopust, V. Vezys, A. L. Marzo, L. Lefrancq, Preferential localization of effector memory cells in nonlymphoid tissue. *Science* **291**, 2413–2417 (2001).
17. B. V. Kumar *et al.*, Human tissue-resident memory T cells are defined by core transcriptional and functional signatures in lymphoid and mucosal sites. *Cell Rep.* **20**, 2921–2934 (2017).
18. C. N. Skon *et al.*, Transcriptional downregulation of S1pr1 is required for the establishment of resident memory CD8+ T cells. *Nat. Immunol.* **14**, 1285–1293 (2013).
19. M. Matloubian *et al.*, Lymphocyte egress from thymus and peripheral lymphoid organs is dependent on S1P receptor 1. *Nature* **427**, 355–360 (2004).
20. E. C. Reilly *et al.*, TRM integrins CD103 and CD49a differentially support adherence and motility after resolution of influenza virus infection. *Proc. Natl. Acad. Sci. U.S.A.* **117**, 12306–12314 (2020).
21. K. D. Zens, J. K. Chen, D. L. Farber, Vaccine-generated lung tissue-resident memory T cells provide heterosubtypic protection to influenza infection. *JCI Insight* **1**, 85832 (2016).
22. N. Iijima, A. Iwasaki, A local macrophage chemokine network sustains protective tissue-resident memory CD4 T cells. *Science* **346**, 93–98 (2014).
23. L. K. Mackay *et al.*, T-box transcription factors combine with the cytokines TGF- β and IL-15 to control tissue-resident memory T cell fate. *Immunity* **43**, 1101–1111 (2015).
24. R. Fonseca *et al.*, Developmental plasticity allows outside-in immune responses by resident memory T cells. *Nat. Immunol.* **21**, 412–421 (2020).
25. J. M. Schenkel *et al.*, Resident memory CD8 t cells trigger protective innate and adaptive immune responses. *Science* **346**, 98–101 (2014).
26. S. Ariotti *et al.*, Skin-resident memory CD8+ T cells trigger a state of tissue-wide pathogen alert. *Science* **346**, 101–105 (2014).
27. F. M. Behr *et al.*, Tissue-resident memory CD8+ T cells shape local and systemic secondary T cell responses. *Nat. Immunol.* **21**, 1070–1081 (2020).
28. S. Cheuk *et al.*, CD49a expression defines tissue-resident CD8+ T cells poised for cytotoxic function in human skin. *Immunity* **46**, 287–300 (2017).
29. S. K. Whitley *et al.*, Local IL-23 is required for proliferation and retention of skin-resident memory TH 17 cells. *Sci. Immunol.* **7**, eabq3254 (2022).
30. S. P. Weisberg *et al.*, Tissue-resident memory T cells mediate immune homeostasis in the human pancreas through the PD-1/PD-L1 pathway. *Cell Rep.* **29**, 3916–3932.e5 (2019).
31. Z. Wang *et al.*, PD-1 hi CD8+ resident memory T cells balance immunity and fibrotic sequelae. *Sci. Immunol.* **4**, eaaw1217 (2019).
32. H. J. Lv *et al.*, Impaired thymic tolerance to α -myosin directs autoimmunity to the heart in mice and humans. *J. Clin. Invest.* **121**, 1561–1573 (2011).
33. M. Delgobo *et al.*, Myocardial milieu favors local differentiation of regulatory T cells. *Circ. Res.* **132**, 565–582 (2023). 10.1161/CIRCRESAHA.122.322183.
34. M. Rieckmann *et al.*, Myocardial infarction triggers cardioprotective antigen-specific T helper cell responses. *J. Clin. Invest.* **129**, 4922–4936 (2019).
35. K. G. Anderson *et al.*, Intravascular staining for discrimination of vascular and tissue leukocytes. *Nat. Protoc.* **9**, 209–222 (2014).
36. S. Sakaguchi *et al.* Annual review of immunology regulatory T cells and human disease. *Ann. Rev. Immunol.* **26**, 541–566 (2020). 10.1146/annurev-immunol-042718.
37. H. Frizzell *et al.*, Organ-specific isoform selection of fatty acid-binding proteins in tissue-resident lymphocytes. *Sci. Immunol.* **5**, eaay9283 (2020).
38. R. Lin *et al.*, Fatty acid oxidation controls CD8+Tissue-resident memory t-cell survival in gastric adenocarcinoma. *Cancer Immunol. Res.* **8**, 479–492 (2020).
39. X. Hua *et al.*, Single-cell RNA sequencing to dissect the immunological network of autoimmune myocarditis. *Circulation* **142**, 384–400 (2020).
40. J. J. Milner *et al.*, Runx3 programs CD8+ T cell residency in non-lymphoid tissues and tumors. *Nature* **552**, 253–257 (2017).
41. D. Wang *et al.*, The transcription factor Runx3 establishes chromatin accessibility of cis-regulatory landscapes that drive memory cytotoxic T lymphocyte formation. *Immunity* **48**, 659–674.e6 (2018).
42. G. C. Baldeviano *et al.*, Interleukin-17A is dispensable for myocarditis but essential for the progression to dilated cardiomyopathy. *Circ. Res.* **106**, 1646–1655 (2010).
43. J. M. Myers *et al.*, Cardiac myosin-Th17 responses promote heart failure in human myocarditis. *JCI Insight* **1**, e85851 (2016).
44. R. Tieu *et al.*, Tissue-resident memory T cell maintenance during antigen persistence requires both cognate antigen and interleukin-15. *Sci. Immunol.* **8**, eadd8454 (2023).
45. C. F. Krebs *et al.*, Pathogen-induced tissue-resident memory TH17 (TRM17) cells amplify autoimmune kidney disease. *Sci. Immunol.* **5**, 4163 (2020).
46. B. V. Kumar, T. J. Connors, D. L. Farber, Human T cell development, localization, and function throughout life. *Immunity* **48**, 202–213 (2018).
47. D. L. Farber, N. A. Yudanin, N. P. Restifo, Human memory T cells: Generation, compartmentalization and homeostasis. *Nat. Rev. Immunol.* **14**, 24–35 (2014).
48. W. Bracamonte-Baran, D. Číháková, Cardiac Autoimmunity: Myocarditis. *Adv. Exp. Med. Biol.* **1003**, 187–221 (2017).
49. D. Číháková *et al.*, Meeting the challenges of myocarditis: New opportunities for prevention, detection, and intervention—a report from the 2021 national heart, lung, and blood institute workshop. *J. Clin. Med.* **11**, 5721 (2022).
50. I. Cabac-Pogorevcic *et al.*, Ischaemic cardiomyopathy. Pathophysiological insights, diagnostic management and the roles of revascularisation and device treatment. Gaps and dilemmas in the era of advanced technology. *Eur. J. Heart Fail.* **22**, 789–799 (2020).
51. A. Mishra, L. Sullivan, M. A. Caligiuri, Molecular pathways: Interleukin-15 signaling in health and in cancer CME staff planners' disclosures acknowledgment of financial or other support. *Clin. Cancer Res.* **20**, 2044–2050 (2014).
52. J. C. Steel, T. A. Waldmann, J. C. Morris, Interleukin-15 biology and its therapeutic implications in cancer. *Trends Pharmacol. Sci.* **33**, 35–41 (2012).
53. B. Jabri, V. Abadie, IL-15 functions as a danger signal to regulate tissue-resident T cells and tissue destruction. *Nat. Rev. Immunol.* **15**, 771 (2015).
54. D. M. Hughes *et al.*, The protective role of GATA6+ pericardial macrophages in pericardial inflammation. *iScience* **27**, 110244 (2024). 10.1016/j.isci.2024.110244.
55. J. F. Deniset *et al.*, Gata6+ pericardial cavity macrophages relocate to the injured heart and prevent cardiac fibrosis. *Immunity* **51**, 131–140.e5 (2019).
56. H. Jin *et al.*, Genetic lineage tracing of pericardial cavity macrophages in the injured heart. *Circ. Res.* **130**, 1682–1697 (2022).
57. D. Číháková, snRNA-Seq of pericardial cells in human cardiomyopathy. Figshare. <https://figshare.com/s/3a2c974f375c9ae6025>. Deposited 25 June 2024.
58. L. K. MacKay *et al.*, The developmental pathway for CD103+ CD8+ tissue-resident memory T cells of skin. *Nat. Immunol.* **14**, 1294–1301 (2013).
59. A. E. Oja *et al.*, Trigger-happy resident memory CD4+ T cells inhabit the human lungs. *Mucosal Immunol.* **11**, 654–667 (2018).
60. P. Hombrink *et al.*, Programs for the persistence, vigilance and control of human CD8+ lung-resident memory T cells. *Nat. Immunol.* **17**, 1467–1478 (2016).
61. A. Cartier, T. Hla, Sphingosine 1-phosphate: Lipid signaling in pathology and therapy. *Science* **366**, eaar5551 (2019).
62. A. J. Bankovich, L. R. Shiow, J. G. Cyster, CD69 suppresses sphingosine 1-phosphate receptor-1 (S1P1) function through interaction with membrane helix 4. *J. Biol. Chem.* **285**, 22328–22337 (2010).
63. A. Bai, H. Hu, M. Yeung, J. Chen, Krüppel-Like Factor 2 Controls T Cell Trafficking by Activating L-Selectin (CD62L) and Sphingosine-1-Phosphate Receptor 1 Transcription 1. *Immunol.* **178**, 7632–7639 (2007).
64. E. M. Steinert *et al.*, Quantifying memory CD8 T cells reveals regionalization of immunosurveillance. *Cell* **161**, 737–749 (2015).
65. H. Wu *et al.*, Pathogenic role of tissue-resident memory T cells in autoimmune diseases. *Autoimmun. Rev.* **17**, 906–911 (2018).
66. M. Künzi, D. Masopust, CD4+ T cell memory. *Nat. Immunol.* **2023**, 1–12 (2023). 10.1038/s41590-023-01510-4.
67. S. N. Mueller, T. Gebhardt, F. R. Carbone, W. R. Heath, Memory T cell subsets, migration patterns, and tissue residence. *Ann. Rev. Immunol.* **31**, 137–161 (2013).
68. B. D. Hondowicz *et al.*, Interleukin-2-dependent allergen-specific tissue-resident memory cells drive asthma. *Immunity* **44**, 155–166 (2016).
69. N. P. Goplen *et al.*, Tissue-resident CD8+ T cells drive age-associated chronic lung sequelae after viral pneumonia. *Sci. Immunol.* **5**, eabc4557 (2020).
70. G. C. Ramosa *et al.*, Myocardial aging as a T-cell-mediated phenomenon. *Proc. Natl. Acad. Sci. U.S.A.* **114**, E2420–E2429 (2017).
71. D. Ashour *et al.*, An interferon gamma response signature links myocardial aging and immunosenescence. *Cardiovasc. Res.* **119**, 2458–2468 (2023).
72. N. Yousef *et al.*, Immune checkpoint inhibitors and cardiovascular toxicity. *Lancet Oncol.* **19**, e447–e458 (2018).
73. K. Chamoto, T. Yaguchi, M. Tajima, T. Honjo, Insights from a 30-year journey: Function, regulation and therapeutic modulation of PD1. *Nat. Rev. Immunol.* **2023**, 1–14 (2023). 10.1038/s41577-023-00867-9.
74. C. S. Boddupalli *et al.*, Interlesional diversity of T cell receptors in melanoma with immune checkpoints enriched in tissue-resident memory T cells. *JCI Insight* **1**, e88955 (2016).
75. F. K. Swirski, M. Nahrendorf, Cardioimmunology: The immune system in cardiac homeostasis and disease. *Nat. Rev. Immunol.* **18**, 733–744 (2018).
76. M. Hulsmans *et al.*, Macrophages facilitate electrical conduction in the heart. *Cell* **169**, 510–522.e20 (2017).
77. H. P. Schultheiss *et al.*, Dilated cardiomyopathy. *Nat. Rev. Dis. Primers* **5**, 1–19 (2019).
78. M. Merlo *et al.*, Evolving concepts in dilated cardiomyopathy. *Eur. J. Heart Fail.* **20**, 228–239 (2018).
79. T. Lampejo, A. Simon, M. Durkin, N. Bhatt, O. Guttmann, Acute myocarditis: Aetiology, diagnosis and management. *Clin. Med.* **21**, 505–515 (2021).
80. M. G. Del Buono *et al.*, Ischemic cardiomyopathy and heart failure after acute myocardial infarction. *Curr. Cardiol. Rep.* **24**, 1505–1515 (2022).
81. A. S. Maisel *et al.*, Adrenergic control of circulating lymphocyte subpopulations effects of congestive heart failure, dynamic exercise, and terbutaline treatment. *J. Clin. Invest.* **85**, 462–467 (1990).
82. T. Tadokoro *et al.*, Acute lymphocytic myocarditis with anti-PD-1 antibody nivolumab. *Circ. Heart Fail.* **9**, e003514 (2016).
83. T. A. Waldmann, The biology of interleukin-2 and interleukin-15: Implications for cancer therapy and vaccine design. *Nat. Rev. Immunol.* **6**, 595–601 (2006).
84. V. Rusinkovich *et al.*, Temporal dynamics of immune response following prolonged myocardial ischemia/reperfusion with and without cyclosporine A. *Acta Pharmacol. Sin.* **40**, 1168–1183 (2019). 10.1038/s41401-018-0197-1.